ACS APPLIED MATERIALS & INTERFACES

Research Article

www.acsami.org

A Sol–Gel Process for Fabrication of $NiO/NiCo_2O_4/Co_3O_4$ Composite with Improved Electrochemical Behavior for Electrochemical Capacitors

Mao-Cheng Liu,[†] Ling-Bin Kong,*[,†,‡] Chao Lu,[†] Xiao-Ming Li,[†] Yong-Chun Luo,[‡] and Long Kang[‡]

[†]State Key Laboratory of Gansu Advanced Non-ferrous Metal Materials and [‡]School of Materials Science and Engineering, Lanzhou University of Technology, Lanzhou 730050, P.R. China

ABSTRACT: Transition metal oxides possess multiple oxidation states that enable rich redox reactions for pseudo capacitanc. They have been investigated as promising electrode materials to achieve high energy density. In this study, $NiO/NiCo_2O_4/Co_3O_4$ composite with high specific surface and mesoporous structure is fabricated by a sol–gel process then calcined at 250 °C. Benefits from the improved electron conductivity and effective mesoporous structure, the fabricated composite exhibits high specific capacitance (1717 F g^{-1}), enhanced rate capability, and excellent electrochemical stability (94.9% retention after 1000 cycles). Interestingly, the specific capacitance of the composite is higher than that of NiO, $NiCo_2O_4$, and Co_3O_4, which indicates a synergistic effect of the composite on improvement of electrochemical performance. The findings demonstrate the importance and great potential of $NiO/NiCo_2O_4/Co_3O_4$ composite in development of high-performance energy-storage systems.

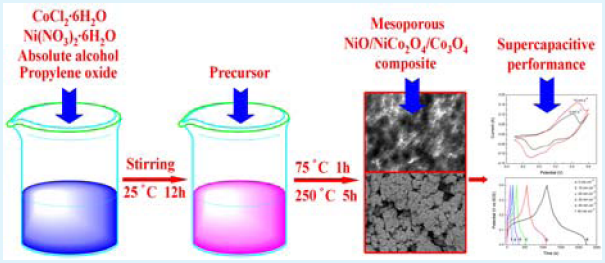

KEYWORDS: *supercapacitor, mesoporous composite, mixed metal oxides, capacitive performance*

1. INTRODUCTION

As energy storage devices having properties intermediate to those of batteries and electrostatic capacitors, electrochemical capacitors (ECs) exhibit the desirable properties of high power density, fast charging, and long cycling life, which make them one of the most promising candidates for next generation power devices.[1−4] ECs, that store energy using either ion adsorption (electrochemical double layer capacitors, EDLCs) or fast surface redox reactions (pseudo capacitors).[5] Energy storage of EDLCs based on ion adsorption at the electrode/electrolyte interface suffered from limited energy density,[6−8] most current research work on ECs has been focused on pseudocapacitors to improve their energy density and make them comparable to batteries.[9,10]

Generally, two main kinds of materials, conducting polymers and metal oxides, have been proposed independently or collaboratively applied in pseudocapacitors.[11−14] Conductive polymers show enhanced capacitive performance, but their specific capacitances are lower than most of metal oxides and poor electrochemical stability need to be further improved.[15−18] Therefore, metal oxides have been considered to be the most promising materials for high-performance pseudocapacitors.[19−21]

As a typical metal oxide electrode material, RuO_2 has a high capacitance, reversible charge/discharge features, and good electrical conductivity, all of which make it the focus of research and development of supercapacitors having the potential to achieve higher energy and power densities.[22,23] Unfortunately, its high cost renders this material unsuitable for commercialized in many applications. Transition metal oxides possess multiple oxidation states/structures that enable rich redox reactions for pseudo capacitance,[24] have been investigated as alternative materials for RuO_2 in next-generation supercapacitors.[25−27] For instance, NiO,[28−30] $NiCo_2O_4$,[23,31,32] and Co_3O_4,[33−35] that have been reported to have high supercapacitive performance, regarding to be the most promising materials for ECs. However, the reported specific capacitance of NiO, $NiCo_2O_4$, and Co_3O_4 were still lower than that of RuO_2, and their capacitive properties also need further enhancement to make them comparable to RuO_2.

NiO, $NiCo_2O_4$, and Co_3O_4 were P-type semiconductors with the band gap of 3.6,[36] 2.1,[37] and 2.2 eV,[38] respectively. Along with mesoporous structure,[39−42] the electrical conductivity[43,44] and the degree of crystallinity[4,45] must be taken into account when predicting the electrochemical performance of these oxides based electrode materials. It is well-known that the electrical conductivity of electrode materials plays a critical role in charge-transfer reactions and internal resistance of the electrodes,[46,47] that can be enhanced by doping with other semiconductors to introduce impurity band effects. The crystallinity of the oxides been considered to determining their electrochemical activity. The proper microstructure will provide high specific surface area as well as good accessibility for the electrolyte.[48−50] For these reasons, it becomes essential to tune microstructure, crystallinity, and electrical conductivity of these oxides based materials for their application in ECs.

Received: June 5, 2012
Accepted: August 27, 2012
Published: August 27, 2012

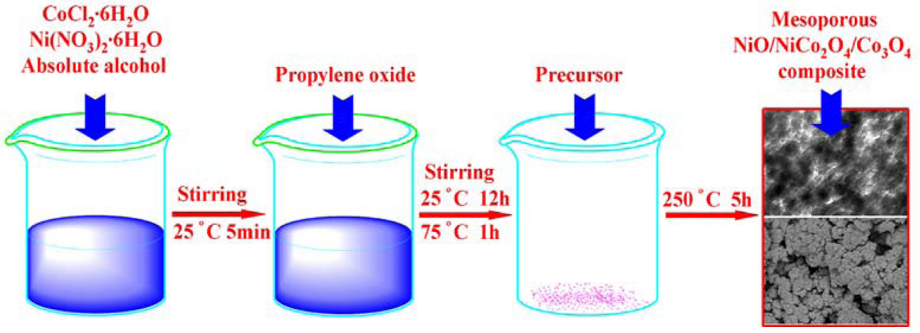

Figure 1. Synthesis procedure for mesoporous $NiO/NiCo_2O_4/Co_3O_4$ composite.

Recently, $MnMoO_4/CoMoO_4$ heterostructured nanowires were fabricated, which exhibit higher performance than single $MnMoO_4$ and $CoMoO_4$ nanowires.[4] What is more, Co_3O_4 nanowire@MnO_2 ultrathin nanosheet core/shell arrays were reported to show excellent pseudocapacitive properties.[51] Both of the researches demonstrate that the fabrication of oxides composite with unique structure is an effective way to improve electrochemical behavior of the electrodes.

In this work, we report a mesoporous $NiO/NiCo_2O_4/Co_3O_4$ composite, which fabricated by a sol−gel process then calcined at 250 °C. The as-prepared composite exhibits a higher specific capacitance than $NiCo_2O_4$, NiO, and Co_3O_4, showing high performance as the electrode material of ECs. On the one hand, this can be attributed to the improved electrical conductivity, low crystallinity, and proper mesoporous structure of the composite. On the other hand, it benefits from feasible oxidation states/structures which contributed by both nickel and cobalt ions. Moreover, the excellent rate capability and cycle stability of the as-prepared material was also demonstrated.

2. EXPERIMENTAL SECTION

2.1. Materials. Analytical grade $CoCl_2·6H_2O$, $Ni(NO_3)_2·6H_2O$, KOH, propylene oxide, and absolute alcohol were purchased from Sinopharm Chemical Reagent Co. Ltd. and used as received without any further purification.

2.2. Fabrication of the $NiO/NiCo_2O_4/Co_3O_4$ Mesoporous Composite. $NiO/NiCo_2O_4/Co_3O_4$ mesoporous composite was synthesized using a modified version of the procedure described in a previous report.[24] The typical preparation process is illustrated in Figure 1: 0.225 g of $Ni(NO_3)_2·6H_2O$ and 0.37 g of $CoCl_2·6H_2O$ were dissolved in 2.5 mL of ethanol and stirred for 5 min, and then 2.0 g of propylene oxide was added and the mixture was stirred at room temperature for another 12 h. The resulting solution was then stirred at 75 °C to promote gelation. The product was dried at 60 °C for 12 h then heated in an air atmosphere at 250 °C for 5 h. The resulting sample was washed with ethanol and distilled water for several times, and then dried at 80 °C for 12 h. For comparison, NiO, $NiCo_2O_4$, and Co_3O_4 were synthesized by the same procedure. The mechanism of gelation can be explained as the following reaction sequence where M

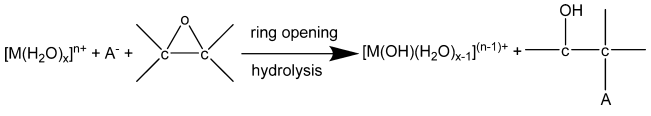

represents nickel or cobalt ions, A^- represents Cl^- or NO_3^- ions. In this procedure, the propylene oxide acts as an acid scavenger through protonation of the epoxide oxygen and subsequent ring-opening by the nucleophilic, anionic conjugate base.[52]

2.3. Structure Characterization. The microstructure and morphology of $NiO/NiCo_2O_4/Co_3O_4$ mesoporous composite was characterized by transmission electron microscope (TEM, JEOL, JEM-2010, Japan) and field-emission scanning electron microscope (SEM, JEOL, JSM-6701F, Japan). The pore properties were investigated by nitrogen adsorption/desorption experiments (ASAP 2020). Crystallite structures were determined by X-ray diffraction (XRD) using a Rigaku D/MAX 2400 diffractometer (Japan) with Cu Kα radiation (λ = 1.5418 Å) operating at 40 kV and 60 mA.

2.4. Electrode Preparation and Electrochemical Measurements. The working electrodes were prepared as follows: 80 wt % $NiO/NiCo_2O_4/Co_3O_4$ was mixed with 7.5 wt % acetylene black and 7.5 wt % conducting graphite in an agate mortar until a homogeneous black powder was obtained. To this mixture was added 5 wt % poly(tetrafluoroethylene), together with a few drops of ethanol. The resulting paste was pressed at 10 MPa into a nickel foam and then dried at 80 °C for 12 h. Each composite electrode contained about 8 mg of electroactive material and had a geometric surface area of about 1 cm^2.

A typical three-electrode glass cell equipped with a working electrode, a platinum foil counter electrode, and a saturated calomel reference electrode (SCE) was used for electrochemical measurements of the as-prepared working electrodes. All electrochemical measurements were performed using an electrochemical working station (CHI660C, Shanghai, China) in 2 M KOH aqueous solution at 25 °C. The corresponding specific capacitance was calculated from the following equation

$$C_m = \frac{C}{m} = \frac{I\Delta t}{\Delta V m} \quad (1)$$

where C_m (F g^{-1}) is the specific capacitance, I (A) is discharge current, Δt (s) is the discharge time, ΔV (V) represents the potential window, and m (g) is the mass of the active material.

3. RESULTS AND DISCUSSION

3.1. Structure Characterization. To determine crystalline phase of the mesoporous $NiO/NiCo_2O_4/Co_3O_4$ composite, we employed XRD measurement. Figure 2 shows XRD patterns of NiO, $NiCo_2O_4$, Co_3O_4, and $NiO/NiCo_2O_4/Co_3O_4$ composite. The presence of the (111), (311), and (400) peak of $NiCo_2O_4$ (JCPDS No. 20−0781) in the patterns of the $NiO/NiCo_2O_4/Co_3O_4$ indicates the existence of the $NiCo_2O_4$ phase. Moreover, the (111) and (012) diffraction peaks of NiO (JCPDS No. 04−0835) as well as (111), (220), (311), (400), (511), and (440) diffraction peaks of Co_3O_4 (JCPDS No. 42−1467) crystal were also appeared in the patterns, means that a $NiO/NiCo_2O_4/Co_3O_4$ composite was successfully fabricated. The lattice parameters of the cubic NiO, $NiCo_2O_4$, and Co_3O_4 crystal, a, were determined from the observed d-spacings by using the formula for a cubic lattice

$$a = d\sqrt{h^2 + k^2 + l^2} \quad (2)$$

dx.doi.org/10.1021/am301010u | ACS Appl. Mater. Interfaces 2012, 4, 4631−4636

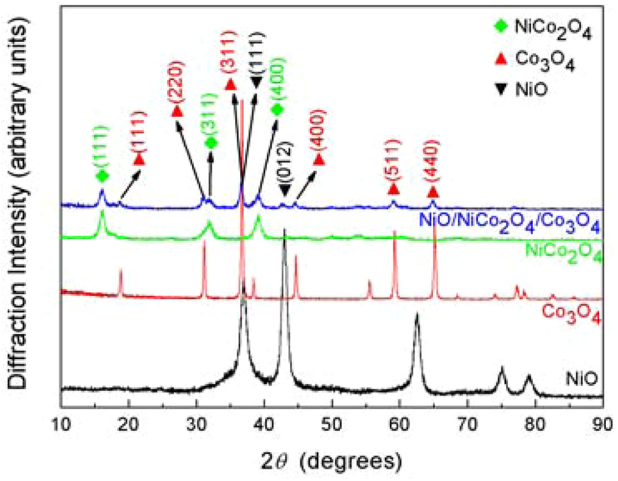

Figure 2. XRD patterns of NiO, Co_3O_4, $NiCo_2O_4$, and NiO/$NiCo_2O_4$/Co_3O_4 composite.

where *h*, *k*, and *l* are the Miller indices. The calculated value of *a*, corresponding to (111) planes of $NiCo_2O_4$, (111) planes of NiO, and (440) planes of Co_3O_4 are 0.8080, 4.209, and 0.8099 nm, which are very close to that of 0.8110, 0.4177, and 0.8034 nm given in the standard PDF card, respectively. The small crystallite size of the NiO/$NiCo_2O_4$/Co_3O_4 nanocrystals is evidenced by the significant broadening of the diffraction peaks in composites pattern compared to that of NiO, $NiCo_2O_4$, and Co_3O_4 crystal patterns, which are favorable for composite to exhibit a high capacitive performance.

Figure 3 shows SEM and TEM images of the NiO/$NiCo_2O_4$/Co_3O_4 composite. A loosely packed porous structure consisting of interconnected nanoparticles, tens nanometers in sizes, was clearly displayed in Figure 3a. This is in accordance with the results of TEM imaging shown in Figure 3b. Figure 3c exhibits the mesoporous structure of the composite with a pore

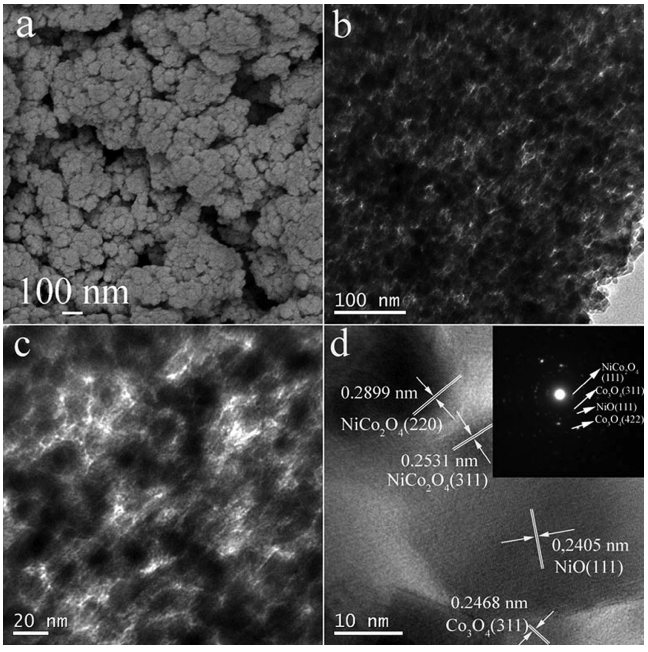

Figure 3. (a) SEM image, (b, c) TEM image, and (d) HRTEM of NiO/$NiCo_2O_4$/Co_3O_4 composite (the inset image is the SAED pattern of NiO/$NiCo_2O_4$/Co_3O_4 composite).

size ranging from 10 to 20 nm. The high-resolution TEM (HRTEM) image shown in Figure 3d reveals the interplanar spacing of the composite. The obtained interplanar spacing of 0.2899 and 0.2531 nm are close to the standard value of 0.2869 and 0.2447 nm for (220) and (311) plane of spinel $NiCo_2O_4$, whereas 0.2405 and 0.2468 nm correspond to (111) plane of cubic NiO and (311) plane of spinel Co_3O_4, respectively. The inseted selected-area electron diffration (SAED) pattern once again confirms the existence of NiO, $NiCo_2O_4$, and Co_3O_4 in the fabricated composite.

The mesoporous characteristics of the composite were further investigated by the N_2 adsorption/desorption isotherms. As can be seen from Figure 4a, the existence of the

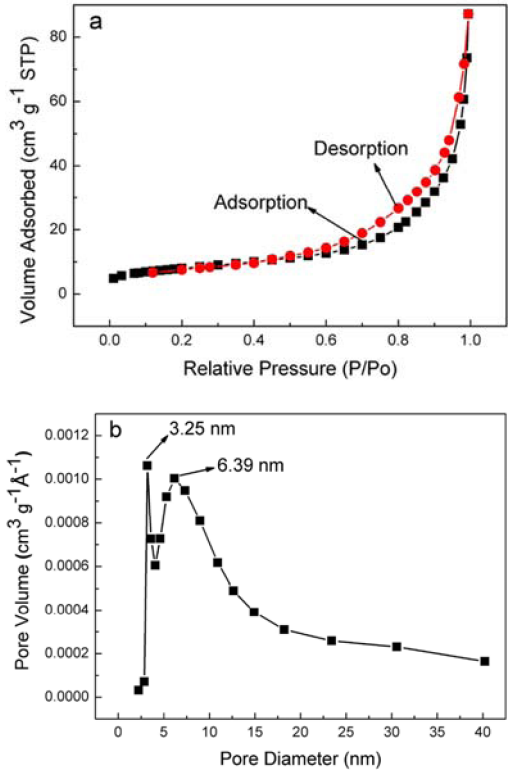

Figure 4. (a) N_2 adsorption/desorption isotherms and (b) pore size distribution curve of the as-fabricated mesoporous NiO/$NiCo_2O_4$/Co_3O_4 composite.

hysteresis loops indicates its porous structure. In Figure 4b, the curve exhibits a narrow pore-size distribution at 3.25 nm and a wide pore size distribution around 6.39 nm, suggesting a hierarchical mesoporous structure. The sample shows a specific surface area of 28.7 $m^2\ g^{-1}$ and an average pore size of 11.4 nm. However, the specific surface area of NiO, $NiCo_2O_4$, and Co_3O_4 are 5.2, 22.7, and 24.6 $m^2\ g^{-1}$, suggesting that the NiO/$NiCo_2O_4$/Co_3O_4 composite shows a higher specific surface area. This is important for the material to serve as a high performance electrode for ECs.

3.2. Electrochemical Characterization. CV, chronopotentiometry, EIS, and cycle measurements were employed to evaluate the electrochemical capacitive performance of the mesoporous NiO/$NiCo_2O_4$/Co_3O_4 composite.

Figure 5a shows the CV of NiO/$NiCo_2O_4$/Co_3O_4 composite at scan rates of 5 and 10 mV s^{-1}. The redox peaks are visible in each voltammogram, indicating that the measured capacitance is mainly based on the redox mechanism. The strong anodic

dx.doi.org/10.1021/am301010u | ACS Appl. Mater. Interfaces 2012, 4, 4631−4636

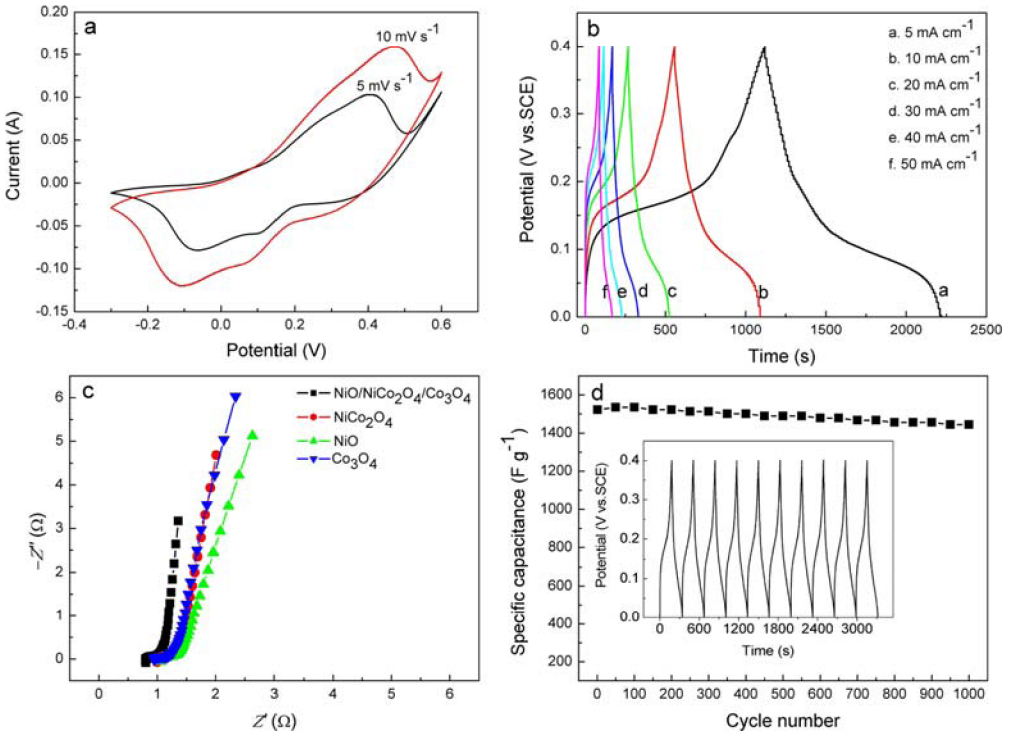

Figure 5. Electrochemical properties of $NiO/NiCo_2O_4/Co_3O_4$ composite. (a) CV curves and (b) charge/discharge curves of the composite. (c) Complex-plane impedance plots of NiO, Co_3O_4, $NiCo_2O_4$, and $NiO/NiCo_2O_4/Co_3O_4$ composite. (d) Cycling performance of the as-fabricated composite (The inset is first ten charge/discharge curves of $NiO/NiCo_2O_4/Co_3O_4$ composite).

peak at 0.40 V (corresponding cathodic peak at 0.09 V) was attributed to the transition of the redox couple Co (II)/Co (III).[53,54] Interestingly, a weak anodic peak appeared at approximately 0.28 V, and the corresponding cathodic peak was at −0.11 V in the CV curve of 10 mV s^{-1}. We consider that this pair of redox peaks was assigned to the redox reactions of Ni (II)/Ni (III). Based on the results of Figure.5a, it is evident that the CV curves of $NiO/NiCo_2O_4/Co_3O_4$ composite display a high redox peak current density. This may be contributed by both nickel and cobalt ions due to their feasible oxidation states/structure in different oxides.[24]

To further calculate the specific capacitance and understand the rate capability of $NiO/NiCo_2O_4/Co_3O_4$ composite electrode. The charge/discharge measurements were performed. Figure 5b shows the charge/discharge curves of the composite electrode at a current density ranging from 5 to 50 mA cm^{-2}. The specific capacitances of the composite electrode, calculated from discharge time according to the eq 1, are1717, 1678, 1600, 1509, 1412, and 1219 F g^{-1} corresponding to the discharging current densities of 5, 10, 20, 30, 40, and 50 mA cm^{-2}, respectively. The specific capacitance gradually decreased at higher current density due to the incremental (IR) voltage drop and the insufficient active material involved in the redox reaction at a higher current densities. However, the as-fabricated composite possesses excellent capacitance at all the current densities evaluated and shows a good rate capability. Even at a high current density of 50 mA cm^{-2}, nearly 75.5% of the initial capacitance value remains. The higher specific capacitance of the $NiO/NiCo_2O_4/Co_3O_4$ composite was due to two factors. First, the improved electron conductivity provides fast charge transfer in the composite. Second, effective mesoporous structure of the composite provides larger surface area and more reaction active sites, which can significantly improve the utilization and the pseudocapacitance of active materials.[54,55]

Figure 5c displays the EIS of NiO, $NiCo_2O_4$, Co_3O_4, and $NiO/NiCo_2O_4/Co_3O_4$ composite electrodes measured at an electrode potential of 0.3 V, respectively. All the impedance spectra were almost similar, being composed of one semicircle component at high-frequency followed by a linear component at the low-frequency. The internal resistance (R_b), which includes the total resistances of the ionic resistance of electrolyte, intrinsic resistance of active materials and contact resistance at the active material/current collector interface, can be obtained from the intercept of the plots on real axis. The semicircle corresponds to the pseudo charge transfer resistance (R_{ct}). The calculated R_b and R_{ct} of the four electrodes are shown in table 1. Obviously, the $NiO/NiCo_2O_4/Co_3O_4$ electrode exhibits lower R_b and R_{ct} than Co_3O_4, NiO, and $NiCo_2O_4$ electrodes due to the improved electron conductivity of the composite. As semiconductors, the band gap of Co_3O_4, NiO, and $NiCo_2O_4$ electrode were various, according to band theory, impurity bands were introduced after these oxides in situ mixed together, thus improving electron conductivity of the composite. At lower frequencies, the straight line represents the diffusive resistance (Warburg impedance) of the electrolyte

Table 1. Internal Resistance (R_b) and Pseudo Charge Transfer Resistance (R_{ct}) of the NiO, $NiCo_2O_4$, Co_3O_4, and $NiO/NiCo_2O_4/Co_3O_4$ Composite Electrodes

samples	R_b (Ω)	R_{ct} (Ω)
$NiO/NiCo_2O_4/Co_3O_4$	0.81	0.1
$NiCo_2O_4$	1.02	0.15
NiO	1.08	0.16
Co_3O_4	0.96	0.13

dx.doi.org/10.1021/am301010u | ACS Appl. Mater. Interfaces 2012, 4, 4631−4636

ions in host materials. Compared with Co_3O_4, NiO, and $NiCo_2O_4$, the $NiO/NiCo_2O_4/Co_3O_4$ composite electrode shows lower Warburg impedance due to its effective mesoporous structure which facilitating electrolyte ions diffusion in the composite.

The excellent cycle stability of the $NiO/NiCo_2O_4/Co_3O_4$ composite electrode at a current density of 20 mA cm^{-2} (2.5 A g^{-1}) is demonstrated in Figure 5d. The specific capacitance increased over the first 50 cycles due to complete activation of the active materials.[17,24] After 50 cycles, the capacitance gradually decreased at higher cycle numbers such that 94.9% of the initial specific capacitance was remained after 1000 cycles. The results reveal the excellent stability of the $NiO/NiCo_2O_4/Co_3O_4$ composite electrode as a high-performance electrode material for pseudo capacitors.

To further illustrate the excellent electrochemical properties and suitability of the synthesized mesoporous $NiO/NiCo_2O_4/Co_3O_4$ composite as an electrode material for ECs, the specific capacitance of NiO, $NiCo_2O_4$, and Co_3O_4 electrodes at a controlled current densities were measured for comparison. Figure 6 shows specific capacitance of NiO, $NiCo_2O_4$, Co_3O_4,

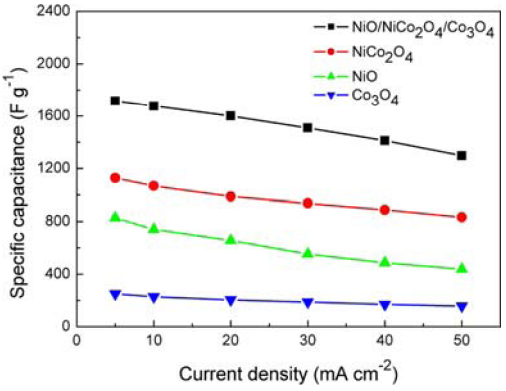

Figure 6. Specific capacitances of Co_3O_4, NiO, $NiCo_2O_4$, and $NiO/NiCo_2O_4/Co_3O_4$ composite at a controlled current density.

and $NiO/NiCo_2O_4/Co_3O_4$ composite, respectively. The specific capacitances of $NiO/NiCo_2O_4/Co_3O_4$ composite are higher than that of NiO, $NiCo_2O_4$, and Co_3O_4, suggesting a higher capacitive performance. The highest specific capacitance, 1717 F g^{-1} at a current density of 5 mA cm^{-2}, is higher than that of 1580 F g^{-1} reported for RuO_2.[57] This specific capacitance is also the highest value reported for nickel and cobalt based oxides materials. Taking advantage of its excellent capacitive performance, low cost, and easy fabrication, the synthesized mesoporous $NiO/NiCo_2O_4/Co_3O_4$ composite is a promising alternative material to RuO_2 in next-generation supercapacitors.

4. CONCLUSION

In summary, mesoporous $NiO/NiCo_2O_4/Co_3O_4$ nanocomposite, a promising and excellent electrode material for electrochemical capacitors is synthesized by a sol–gel process followed by calcining at 250 °C. It exhibits a high specific capacitance, excellent rate capability, and good cycle stability. A high specific capacitance of 1717 F g^{-1} was achieved at a current density of 5 mA cm^{-2} and 94.9% of the initial specific capacitance was remained after 1000 cycles. The excellent electrochemical capacitive performance, low cost, and easy fabrication of the as-prepared mesoporous $NiO/NiCo_2O_4/Co_3O_4$ composite render it a promising electrode material for electrochemical capacitors.

AUTHOR INFORMATION

Corresponding Author

*Tel.: +86-931-2976579. Fax: +86-931-2976578. E-mail: konglb@lut.cn.

Notes

The authors declare no competing financial interest.

ACKNOWLEDGMENTS

This work was supported by the National Natural Science Foundation of China (21163010), the Key Project of Chinese Ministry of Education (212183), and the Natural Science Funds for Distinguished Young Scholars of Gansu Province (1111RJDA012).

REFERENCES

(1) Miller, J. R.; Outlaw, R. A.; Holloway, B. C. *Science* **2010**, *329*, 1637–1369.
(2) Pech, D.; Brunet, M.; Durou, H.; Huang, P.; Mochalin, V.; Gogotsi, Y. *Nat. Nanotechnol.* **2010**, *5*, 651–654.
(3) Brezesinski, T.; Wang, J.; Tolbert, S. H.; Dunn, B. *Nat. Mater.* **2010**, *9*, 146–151.
(4) Mai, L. Q.; Yang, F.; Zhao, Y. L.; Xu, X.; Xu, L.; Luo, Y. Z. *Nat. Commun.* **2011**, *2*, 381–385.
(5) Ania, C. O.; Khomenko, V.; Raymundo-Pinero, E.; Parra, J. B.; Beguin, F. *Adv. Funct. Mater.* **2007**, *17*, 1828–1836.
(6) Reddy, A. L. M.; Shaijumon, M. M.; Gowda, S. R.; Ajayan, P. M. *J. Phys. Chem. C* **2010**, *114*, 658–663.
(7) Qu, Q. T.; Yang, S. B.; Feng, X. L. *Adv. Mater.* **2011**, *23*, 5574–5580.
(8) Zhou, W. W.; Liu, J. P.; Chen, T.; Tan, K. S.; Jia, X. T.; Luo, Z. Q.; Cong, C. X.; Yang, H. P.; Li, C. M.; Yu, T. *Phys. Chem. Chem. Phys.* **2011**, *13*, 14462–14465.
(9) Chen, W.; Fan, Z. L.; Gu, L.; Bao, X. H.; Wang, C. L. *Chem. Commun.* **2010**, *46*, 3905–3907.
(10) Bae, J.; Song, M. K.; Park, Y. J.; Kim, J. M.; Liu, M. L.; Wang, Z. L. *Angew. Chem., Int. Ed.* **2011**, *50*, 1683–1687.
(11) Wu, Z. S.; Wang, D. W.; Ren, W. C.; Zhao, J. P.; Zhou, G. M.; Li, F.; Cheng, H. M. *Adv. Funct. Mater.* **2010**, *20*, 3595–3602.
(12) Kotz, R.; Carlen, M. *Electrochim. Acta* **2000**, *45*, 2483–2498.
(13) Huang, J. S.; Sumpter, B. G.; Meunier, V. *Angew. Chem., Int. Ed.* **2008**, *47*, 520–524.
(14) Lang, J. W.; Yan, X. B.; Xue, Q. J. *J. Power Sources* **2011**, *196*, 7841–7846.
(15) Ding, S. J.; Zhu, T.; Chen, J. S.; Wang, Z. Y.; Yuan, C. L.; Lou, X. W. *J. Mater. Chem.* **2011**, *21*, 6602–6606.
(16) Wang, H. L.; Casalongue, H. S.; Liang, Y. Y.; Dai, H. J. *J. Am. Chem. Soc.* **2010**, *132*, 7472–7477.
(17) Kong, L. B.; Liu, M. C.; Lang, J. W.; Liu, M.; Luo, Y. C.; Kang, L. *J. Solid State Electrochem.* **2011**, *15*, 571–577.
(18) Hulicova-Jurcakova, D.; Kodama, M.; Shiraishi, S.; Hatori, H.; Zhu, Z. H.; Lu, G. Q. *Adv. Funct. Mater.* **2009**, *19*, 1800–1809.
(19) Kong, L. B.; Lang, J. W.; Liu, M.; Luo, Y. C.; Kang, L. *J. Power sources* **2009**, *194*, 1194–1201.
(20) Wang, G. X.; Shen, X. P.; Horvat, J.; Wang, B.; Liu, H.; Wexler, D.; Yao, J. *J. Phys. Chem. C* **2009**, *113*, 4357–4361.
(21) Lee, J. K.; Kim, G. P.; Kim, K. H.; Song, I. K.; Baeck, S. H. *J. Nanosci. Nanotechnol.* **2010**, *10*, 3676–3679.
(22) Sugimoto, W.; Iwata, H.; Yasunaga, Y.; Murakami, Y.; Takasu, Y. *Angew. Chem., Int. Ed.* **2003**, *42*, 4092–4096.
(23) Lee, C. Y.; Bond, A. M. *Langmuir* **2010**, *26*, 16155–16162.
(24) Wei, T. Y.; Chen, C. H.; Chien, H. C.; Lu, S. Y.; Hu, C. C. *Adv. Mater.* **2010**, *22*, 347–351.
(25) Wang, H. Q.; Yang, G. F.; Li, Q. Y.; Zhong, X. X.; Wang, F. P.; Li, Z. S.; Li, Y. H. *New J. Chem.* **2011**, *35*, 469–475.

(26) Yuan, C. Z.; Zhang, X. G.; Su, L. H.; Gao, B.; Shen, L. F. *J. Mater. Chem.* **2009**, *19*, 5772−5777.
(27) Hashem, A. M.; Abuzeid, H. M.; Abdel-Ghany, A. E.; Mauger, A.; Zaghib, K.; Julien, C. M. *J. Power sources* **2012**, *202*, 291−298.
(28) Lang, J. W.; Kong, L. B.; Wu, W. J.; Luo, Y. C.; Kang, L. *Chem. Commun.* **2008**, *35*, 4213−4215.
(29) Yang, H. B.; Guai, G. H.; Guo, C. X.; Song, Q. L.; Jiang, S. P.; Wang, Y. L.; Zhang, W.; Li, C. M. *J. Phys. Chem. C* **2011**, *115*, 12209−12215.
(30) Lu, Q.; Lattanzi, M. W.; Chen, Y. P.; Kou, X. M.; Li, W. F.; Fan, X.; Unruh, K. M.; Chen, J. G.; Xiao, J. Q. *Angew. Chem., Int. Ed.* **2011**, *50*, 6847−6850.
(31) Wu, Y. Q.; Chen, X. Y.; Ji, P. T.; Zhou, Q. Q. *Electrochim. Acta* **2011**, *56*, 7517−7522.
(32) Wang, H. W.; Hu, Z. A.; Chang, Y. Q.; Chen, Y. L.; Wu, H. Y.; Zhang, Z. Y.; Yang, Y. Y. *J. Mater. Chem.* **2011**, *21*, 10504−10511.
(33) Fan, Y. Q.; Shao, H. B.; Wang, J. M.; Liu, L.; Zhang, J. Q.; Cao, C. N. *Chem. Commun.* **2011**, *47*, 3469−3471.
(34) Wang, D. W.; Wang, Q. H.; Wang, T. M. *Inorg. Chem.* **2011**, *50*, 6482−6492.
(35) Wang, H. T.; Zhang, L.; Tan, X. H.; Holt, C. M. B.; Zahiri, B.; Olsen, B.; Mitlin, C. D. *J. Phys. Chem. C* **2011**, *115*, 17599−17605.
(36) Choi, J. M.; Im, S. *Appl. Surf. Sci.* **2005**, *244*, 435−438.
(37) Hu, L. F.; Wu, L. M.; Liao, M. Y.; Fang, X. S. *Adv. Mater.* **2011**, *23*, 1988−1992.
(38) Kumar, R. V.; Diamant, Y.; Gedanken, A. *Chem. Mater.* **2000**, *12*, 2301−2305.
(39) Tian, Z. R.; Tong, W.; Wang, J. Y.; Duan, N. G.; Krishnan, V. V.; Suib, S. L. *Science* **1997**, *276*, 926−930.
(40) Rao, Y.; Antonelli, D. M. *J. Mater. Chem.* **2009**, *19*, 1937−1944.
(41) Cabo, M.; Pellicer, E.; Rossinyol, E.; Estrader, M.; Lopez-Ortega, A.; Nogues, J.; Castell, O. E.; Surinach, S.; Baro, M. D. *J. Mater. Chem.* **2010**, *20*, 7021−7028.
(42) Dai, M. Z.; Song, L. Y.; LaBelle, J. T.; Vogt, B. D. *Chem. Mater.* **2011**, *23*, 2869−2878.
(43) Lee, J. W.; Ahn, T.; Soundararajan, D.; Ko, J. M.; Kim, J. D. *Chem. Commun.* **2011**, *47*, 6305−6307.
(44) Sassoye, C.; Laberty, C.; Khanh, H. L.; Cassaignon, S.; Boissiere, C.; Antonietti, M.; Sanchez, C. *Adv. Funct. Mater.* **2009**, *19*, 1922−1929.
(45) Liu, J. P.; Li, Y. Y.; Huang, X. T.; Li, G. Y.; Li, Z. K. *Adv. Funct. Mater.* **2008**, *18*, 1448−1458.
(46) Zhao, D. D.; Zhou, W. J.; Li, H. L. *Chem. Mater.* **2007**, *19*, 3882−3891.
(47) Yang, G. W.; Xu, C. L.; Li, H. L. *Chem. Commun.* **2008**, *48*, 6537−6539.
(48) Fertig, N.; George, M.; George, M.; Blick, R. H.; Behrends, J. C. *Appl. Phys. Lett.* **2002**, *81*, 4865−4867.
(49) Fu, G. R.; Hu, Z. A.; Xie, L. J.; Jin, X. Q.; Xie, Y. L.; Wang, Y. X.; Zhang, Z. Y.; Yang, Y. Y.; Wu, H. Y. *Int. J. Electrochem. Sci.* **2009**, *4*, 1052−1062.
(50) Kim, J. H.; Kang, S. H.; Zhu, K.; Kim, J. Y.; Neale, N. R.; Frank, A. J. *Chem. Commun.* **2011**, *47*, 5214−5216.
(51) Liu, J. P.; Jiang, J.; Cheng, C. W.; Li, H. G.; Zhang, J. X.; Gong, H.; Fan, H. J. *Adv. Mater.* **2011**, *23*, 2076−2081.
(52) Cui, H. T.; Zayat, M.; Levy, D. *J. Sol−Gel Sci. Technol.* **1990**, *35*, 175−181.
(53) Singh, R. N.; Koenig, J. F.; Poillerat, G.; Chartier, P. *J. Electrochem. Soc.* **1990**, *137*, 1408−1413.
(54) Singh, R. N.; Hamdani, M.; Koenig, J. F.; Poillerat, G.; Gautier, J. L.; Chartier, P. *J. Appl. Electrochem.* **1990**, *20*, 442−446.
(55) Liang, K.; Tang, X. Z.; Hu, W. C. *J. Mater. Chem.* **2012**, *22*, 11062−11067.
(56) Liu, C.; Li, F.; Ma, L. P.; Cheng, H. M. *Adv. Mater.* **2010**, *22*, E28−E62.
(57) Hu, L. F.; Wu, L. M.; Liao, M. Y.; Fang, X. S. *Adv. Mater.* **2011**, *23*, 1988−1992.